

NUMERICAL STUDIES ON RESIDUAL STRENGTH OF DENTED TENSION LEG PLATFORMS UNDER COMPRESSIVE LOAD

Quang Thang Do^{a,*}, Van Nhu Huynh^a, Dinh Tu Tran^a

^a*Faculty of Transportation Engineering, Nha Trang University, 02 Nguyen Dinh Chieu street, Nha Trang city, Khanh Hoa province, Vietnam*

Article history:

Received 11/06/2020, Revised 04/08/2020, Accepted 07/08/2020

Abstract

This paper focuses on numerical investigations and derived formulation to evaluate the residual strength of tension leg platforms (TLPs) with the local denting damage under axial compression loading. The damage generation scenarios in this research are represented the collision accidents of offshore stiffened cylinders TLPs with supply ships or floating subjects. The finite element model is performed using a commercial software package ABAQUS, which has been validated against the experiments from the authors and other researchers. Case studies are then performed on design examples of LTPs when considering both intact and damaged conditions. Based on the rigorous numerical results, the new simple design formulations to predict residual strength of dented TLPs are derived through a regression study as the function of a non-dimensional dent depth. The accuracy and reliability of the derived formulation are validated by comparing it with the available test results in the literature. A good agreement with existing test data for ship-offshore structure collisions is achieved.

Keywords: dented stringer-stiffened cylinder; residual strength; tension leg platforms (LTPs); axial compression; residual strength formulation.

[https://doi.org/10.31814/stce.nuce2020-14\(3\)-09](https://doi.org/10.31814/stce.nuce2020-14(3)-09) © 2020 National University of Civil Engineering

1. Introduction

In the field of marine structures, tension leg platforms (TLPs) have been widely adopted as compression structures for floating offshore installation of oil production and drilling industry. Recently, the application is also used in the floating breakwater system, the fish-farming cage system, as well as buoyancy columns of floating offshore wind turbine foundations. TLPs are floating structures of semi-submersible type and moored by vertical tendons under initial pretension imposed by excess buoyancy. They are applied in deep oceans (larger than 200-300 m) and position restrained by a set of taut moored tethers. The buoyant legs are usually designed as orthogonally stiffened cylindrical shells with stringers and ring frames to resist the hydrostatic pressure and axial force. Ring-stiffeners are very effective at strengthening cylindrical shells against external pressure loading. Stringers (longitudinal stiffeners) are normally used to provide additional stiffness in the axially compressed members.

During their operation life-cycle, TLPs are not only worked under the operational loads arising from extreme ocean conditions of the environment but also exposed to accidental events which may

*Corresponding author. *E-mail address:* thangdq@ntu.edu.vn (Do, Q. T.)

involve ship collision, impact by falling objects from platform decks, fire, and explosions. One of the important accidents is involved ship collisions which have been highlighted to be the most significant cause of damaged offshore structures. Although the consequences of most of the offshore collisions have been illustrated to date, this type of event is of a serious character that will endanger human life and cause financial losses [1]. A typically damaged column of a platform is shown in Fig. 1. Moreover, the cost of extensive repair work of such damage can be significantly expensive because of economic and technical reasons, immediate repair of the damage is difficult and sometimes impossible [2]. Recently, ship collisions with TLPs are one of the key design considerations for evaluating of TLPs performance and safety. Therefore, efficient and accurate assessment methods for evaluating the effect of the damage are vital for decision making. The operators need to decide the immediate repair actions by evaluating the effects of the damage on the safety of the platform through residual strength assessment procedure [3].



Figure 1. Damaged platform column [3]

In operation, TLPs members must carry significant axial loads from the deck down while also resisting hydrostatic external pressure. Based on the availability of a large database of reported experiments and design guides for ultimate strength tests on intact fabricated stringer and /or ring-stiffened cylinders, the case of intact cylinder buckling in offshore structures is well understood [4–8]. However, the residual strength of dented stiffened cylinders is investigated relatively in few studies and there is a limited database of experiments by Ronalds and Dowling [9], Harding and Onoufriou [10]; Walker et al. [11, 12]. Additionally, Do et al. [13] conducted the dynamic mass impact tests on two stringer-stiffened cylinders (denoted as SS-C-1 and SS-C-2) with local impact at mid-span. These models were then performed under hydrostatic pressure for assessing the residual strength of these structures after collision [14]. Furthermore, the details of numerical analysis of the TLPs were provided in references [15–19]. In these references, the case studies were also presented for evaluating the impact response of stringer-stiffened cylinders, for example, the strain-rate hardening effects, the effect of impact locations, the effect of stringer-stiffeners as well as effect of striker header shapes. However, the case studies were only performed on small-scale stringer-stiffened cylinders. Recently, Do et al. [20] and Cho et al. [21] provided details of four ring-stiffened cylinders, namely, RS-C-1, RS-C-2, RS-C-3, and RS-C-4. The model had seven bays and separated by six flat-bar ring-stiffeners. The damages were performed by the free-fall testing frame and their residual strengths were tested under hydrostatic pressure.

Nowadays, nonlinear finite element methods (NFEM) are great tools to forecast ship and offshore cylinder structural collisions. It is also the convenience and economic efficiency to perform the full

scale of reality structures where all boundary conditions and material properties can be included [19–22]. Therefore, the best way to evaluate the ultimate strength after collisions between ship and offshore cylinders is carefully performed the NFEM.

The idea of the present study is to systematically investigate the behavior of dented LTPs under axial compression by using finite element software package ABAQUS. Then, parametric studies are performed on design examples of LTPs for assessing the factors of the reduction in ultimate strength and to clarify the progressive collapse responses. Based on the rigorous numerical results, the new simple design formulations to predict residual strength of dented TLPs are derived through a regression study as the function of a non-dimensional dent depth.

2. Case studies

In this section, the residual strength of the damaged stringer-stiffened cylinder with T-shaped ring-stiffeners and L-shaped stringer stiffeners is now studied under axial compressive loads. The model is a design example of a stringer-stiffened cylindrical shell of the TLPs design concepts given in ABS (2018) [23]. The dimensions and material properties of the model are listed in Table 1.

Table 1. Properties of the stringer-stiffened cylinder considered in case study

Property	Symbol	Value
Cylinder radius (mm)	R	4200
Shell thickness (mm)	t	20
Ring-stiffener spacing (mm)	L_S	3500
Total cylinder length (mm)	L	10500
Number of ring-stiffeners	n_r	2
Ring-stiffener web height (mm)	h_{rw}	700
Ring-stiffener web thickness (mm)	t_{rw}	12
Ring-stiffener flange width (mm)	b_{rf}	300
Ring-stiffener flange thickness (mm)	t_{rf}	16
Number of stringer-stiffeners	n_s	36
Stringer-stiffener web height (mm)	h_{sw}	250
Stringer-stiffener web thickness (mm)	t_{sw}	12
Stringer-stiffener flange width (mm)	w_{st}	90
Stringer-stiffener flange thickness (mm)	t_{sf}	12
Yield strength (MPa)	σ_Y	355
Young's modulus (GPa)	E	206
R/t	R/t	210

2.1. Finite element modelling

It is noted that the accuracy and reliability of developed numerical techniques have been validated and given in references [15–21, 24] by the author. Therefore, in this study, the numerical method is only focused on the explanation of case study models. Nonlinear finite element analyses were performed by using the explicit solution of the ABAQUS software. All structures were modeled by shell element S4R. These element types are hourglass control and decreased the time integration. The

striker was modeled as rigid body with R3D4 element type. The contact between striker header shape and cylindrical shell surface was determined by general contact with penalty approach. The friction coefficient at contact area was defined with 0.3 [24].

Before performing the numerical simulations on test model, the convergence tests were carried out to choose the optimum mesh size. The mesh size of the contact zone was 40×40 mm, while that for the out of the contact zone was 80×80 mm. This mesh size is sufficiently fine for recording the local denting response precisely. For the boundary conditions, the ends of both thick support structures of the model were restrained in all degrees. The full geometry and boundary conditions of each model are provided in the finite element modelling, as shown in Fig. 2.

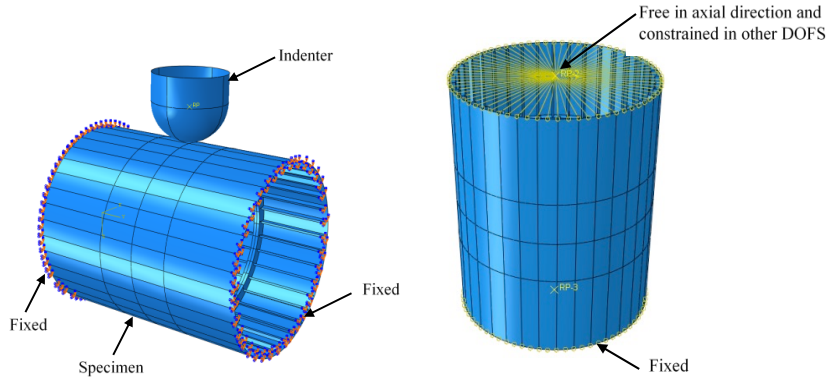


Figure 2. Finite element analysis setup for inducing damage to specimens and post-damage collapse analysis

2.2. Material properties

In collision analysis, the material properties were applied using the revised equations reported in reference Do et al. [13]. These equations were developed using the rigorous dynamic tensile test results on different steels. The equations from (1) to (5) were applied to consider the yield plateau and strain hardening. The effect of strain-rate hardening was also included by using Eqs. (6) to (9). In this paper, the range of strain rates was performed with 10/s, 20/s, 50/s, 70/s, 100/s, to 150/s. It is noted that the maximum strain rate in numerical results was 48.9/s. Therefore, the range of strain rates was suitable for covering all cases of numerical results.

$$\sigma_{tr} = E\varepsilon_{tr} \quad \text{when } 0 < \varepsilon_{tr} \leq \varepsilon_{Y,tr} \quad (1)$$

$$\sigma_{tr} = \sigma_{Y,tr} + (\sigma_{HS,tr} - \sigma_{Y,tr}) \frac{\varepsilon_{tr} - \varepsilon_{Y,tr}}{\varepsilon_{HS,tr} - \varepsilon_{Y,tr}} \quad \text{when } \varepsilon_{Y,tr} < \varepsilon_{tr} \leq \varepsilon_{HS,tr} \quad (2)$$

$$\sigma_{tr} = \sigma_{HS,tr} + K(\varepsilon_{tr} - \varepsilon_{HS,tr})^n \quad \text{when } \varepsilon_{HS,tr} < \varepsilon_{tr} \quad (3)$$

where

$$n = \frac{\sigma_{T,tr}}{\sigma_{T,tr} - \sigma_{HS,tr}} (\varepsilon_{T,tr} - \varepsilon_{HS,tr}) \quad (4)$$

$$K = \frac{\sigma_{T,tr} - \sigma_{HS,tr}}{(\varepsilon_{T,tr} - \varepsilon_{HS,tr})^n} \quad (5)$$

$$\frac{\sigma_{YD}}{\sigma_Y} = 1 + 0.3 \left(\frac{E}{1000\sigma_Y} \right)^{0.5} (\dot{\varepsilon})^{0.25} \quad (6)$$

$$\frac{\sigma_{YD}}{\sigma_Y} = 1 + \left[0.16 \left(\frac{\sigma_T}{\sigma_{YD}} \right)^{3.325} (\dot{\epsilon})^{1/15} \right]^{0.35} \quad (7)$$

$$\frac{\sigma_{YD}}{\sigma_Y} = 1 + \left[0.16 \left(\frac{\sigma_T}{\sigma_{YD}} \right)^{3.325} (\dot{\epsilon})^{1/15} \right]^{0.35} \quad (8)$$

$$\frac{\varepsilon_{TD}}{\varepsilon_T} = 1 - 0.117 \left[\left(\frac{E}{1000\sigma_Y} \right)^{2.352} \left(\frac{\sigma_T}{\sigma_Y} \right)^{0.588} \right] \quad (9)$$

where $\sigma_{tr}, \varepsilon_{tr}$ are true stress and strain, respectively; $\sigma_{Y,tr}, \sigma_{HS,tr}, \sigma_{T,tr}$ are true yield strength, true hardening start stress and true ultimate tensile strength, respectively; $\varepsilon_{HS,tr}, \varepsilon_{T,tr}$ are true hardening start strain and true ultimate tensile strain, respectively; σ_{TD}, σ_{YD} are dynamic ultimate tensile strength and dynamic yield strength, respectively; $\varepsilon_T, \varepsilon_{TD}$ are ultimate tensile strain and dynamic ultimate tensile strain, respectively; $\varepsilon_{HSD}, \varepsilon_{HSS}$ are dynamic hardening start strain and static hardening start strain, respectively; $\varepsilon_Y, \dot{\epsilon}$ are yield strain and equivalent strain rate, respectively.

2.3. Residual stresses and initial imperfections

As in the current cases, the simulations consisted of two steps: first, inducing damage and second, post-damage collapse analysis under compression. Before proceeding to the first analysis step, initial imperfections were inputted into the models. The best solution is inputted directly measurement imperfection values into modeling models. Because this data not only considering local buckling mode but also including overall buckling mode. Therefore, the collapse shapes were correlated between numerical and experimental results. However, if the measurement imperfection data did not provide, it could be used some formulations and assumptions to determine the imperfection magnitudes. For this goal, it was performed using eigenvalue buckling analyses. In general, the first eigenvalue buckling mode was selected as the initial imperfection shape. In the eigenvalue buckling analysis, fixed boundary conditions at both cylinder ends were assumed. These values were considered when determining the imperfection magnitude associated with the eigenvalue buckling mode. The problem is how large imperfection magnitude was introduced. For this purpose, Das et al. [25] considered determining the magnitude of imperfection associated with the eigenvalue buckling modes by comparing numerically-obtained ultimate strength values with the ones calculated using the ultimate strength formulations. The maximum of initial imperfection magnitude was obtained approximate 0.5 times of cylinder's thickness. Additionally, the maximum initial imperfection magnitude values were 0.5% of the cylinder radius R , which corresponded to the upper limit of tolerable imperfection for stringer-stiffened cylinders by API [26]. Teguh et al. [8] determined the initial imperfection approximately $0.4t$ (t is shell thickness) after comparing the numerical results and test results of small-scaled cylinder models. In this study, the imperfection magnitude was determined with approximated $0.5t$ [8, 25, 26]. For considering the local buckling and overall buckling modes, the combination of the first and sixth eigen buckling modes was obtained [8, 27], as shown in Fig. 3. It is noted that combination of the first and sixth eigen buckling modes was selected by evaluation of the failure modes criteria under basic parameters (shell thickness, overall length, stiffener height, stiffener spacing and cylinder radius).

During the manufacturing processes, stiffened cylinder was exposed by cold bending and welding procedures. It is evident that residual stresses from cold bending and welding procedures were significantly affected by the strength of final structures [14]. Therefore, these residual stresses should be considered in numerical modelling. In this study, both residual stresses from cold bending and welding have been included in numerical analysis, as illustrated in Figs. 4 to 6. The summary of numerical

procedures is shown in Fig. 7. Furthermore, the comparison of collapsed shape between an intact case and damaged case with $R/t = 210$ was described in Fig. 8. It is clear that the collapsed shape of the intact model seems to be symmetry while that of damaged model is asymmetry. However, the damaged area of dented case is larger than of an intact case. Because of lack of symmetry in the cross-section of the dented cylinder, the axial stress produced by axial compression applied eccentrically causing an additional moment with respect to the middle surface of the wall. In damaged condition, contrary to the intact case, earlier buckling leads to a decrease in stiffness, followed by collapse after the ultimate strength was reached. The ultimate strength was not reduced to any great extent, as the dent depth increased. The increase in the dent depth did not appreciably alter the end-shortening response.

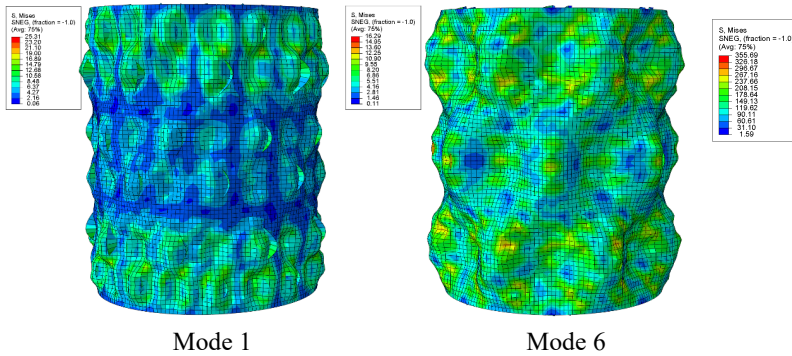


Figure 3. Buckling modes

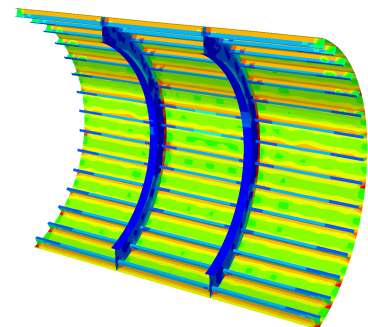


Figure 4. Welding residual stress distribution

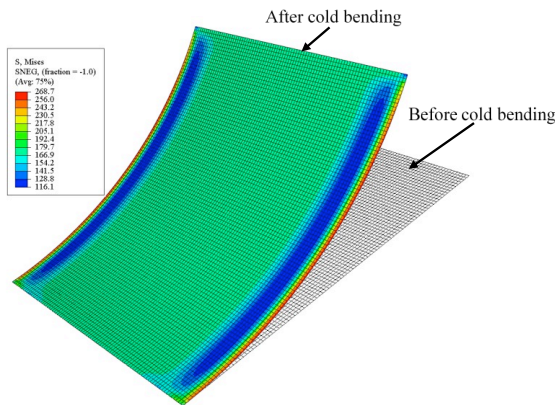


Figure 5. Contour plot of residual stress of typical plate after cold bending

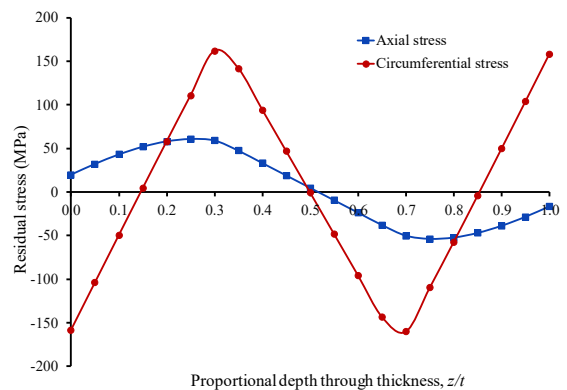


Figure 6. Cold bending residual stress distribution for the model

2.4. Effect of impact velocity

In this section, the effect of impact velocities was investigated by increasing the initial impact velocity with 2.0 m/s, 4.0 m/s, 6.0 m/s, 8.0 m/s, 10 m/s and 15 m/s. The striking mass was assumed as 100 tons with hemisphere indenter type. It is evident that the impact energy was proportional to the square of impact velocity v . Moreover, the strain rate is also linearly proportional to impact velocity v . The patterns of deformation during impact processes are indicated in Fig. 9. The magnitudes of dent

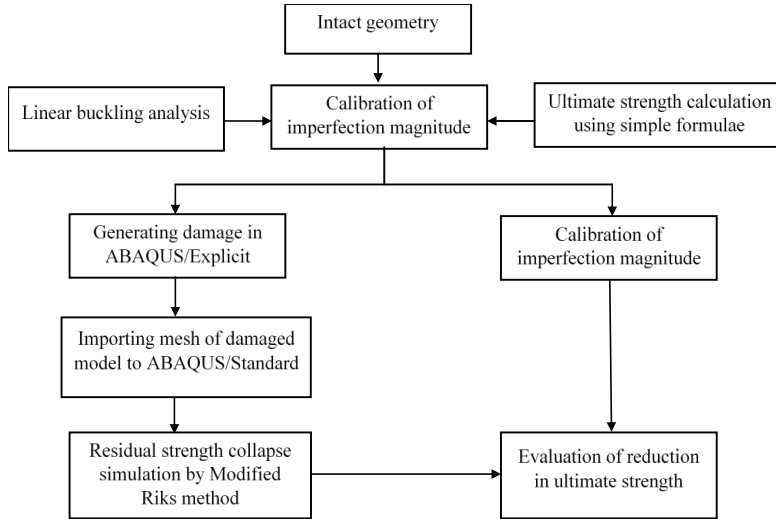


Figure 7. Procedures for assessment of residual strength of TLPs under compression loadings

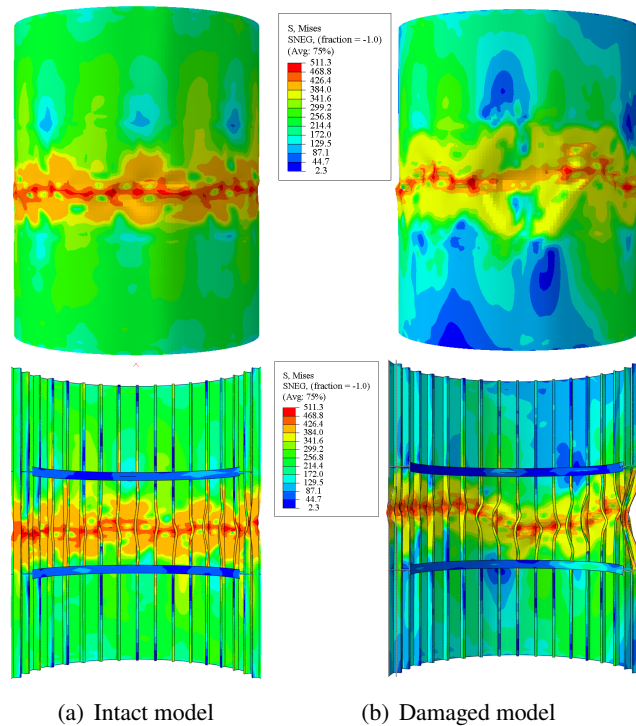


Figure 8. Collapsed shape of stringer-stiffened cylinder model ($R/t = 210$)

depth were increased gradually from $d = 0$ mm (intact model) until maximum dent depth $d = 730$ mm. After generating the impact damage, the models were consequently subjected to compressive load. In the post-damage collapse analysis, the modified Riks method was used. The material was assumed to be elastic-perfect plastic. The typical deformation progress under axial compression load of model was described in Fig. 10.

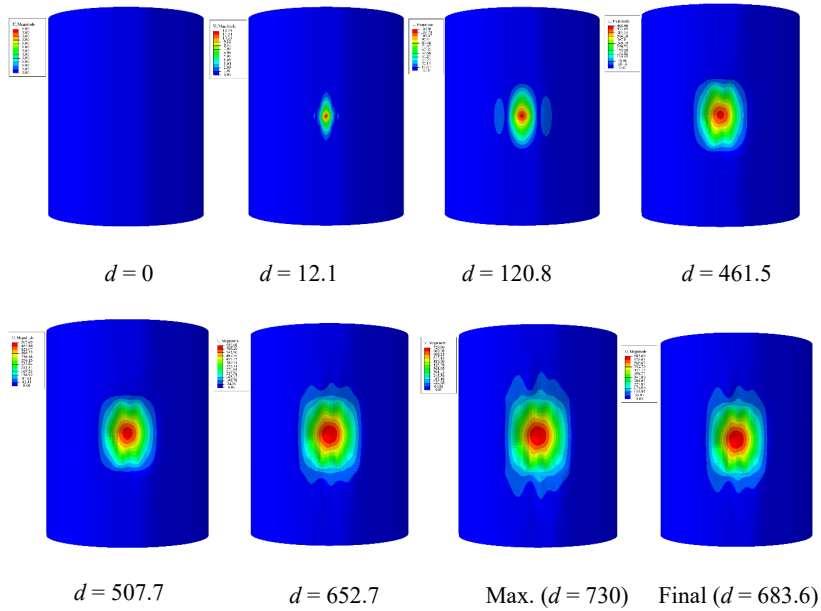


Figure 9. Typical deformation progress under collision load of model (units: mm)

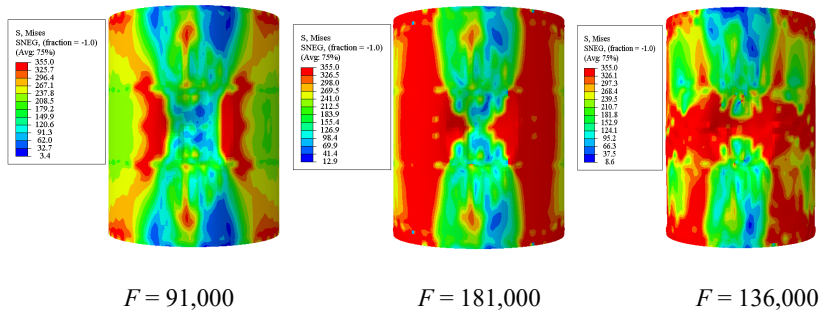


Figure 10. Typical deformation progress under axial compression load (units: kN)

The reduction of ultimate strength with various velocities when compared to intact model was shown in Fig. 11. It is clear that the ultimate strength reduction is not significantly owing to the sturdiness of the stringers, and in the worst case, it is not more than 15%.

2.5. Effect of collision zone location

It is clear that the extent of local denting damage of the stiffened cylinder was strongly dependent on the impact locations. Furthermore, permanent dent depth was also significantly decreased with each location in the longitudinal direction of stiffened cylinder. The maximum permanent dent depth was located at the mid-length of the cylinder, and it was decreased gradually to boundary conditions. However, the reduction of ultimate strength with various impact locations was not rapidly decreased as maximum permanent dent depth. The force-axial shortening relation curve with various impact locations can be seen in Fig. 12. The maximum ultimate strength reduction has occurred at mid-bay of ring stiffeners with 7% when compared to impact location near boundary conditions.

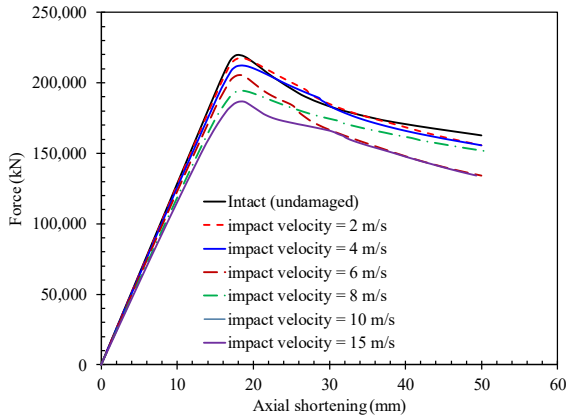


Figure 11. Force-axial shortening relation curve of model ($R/t = 210$)

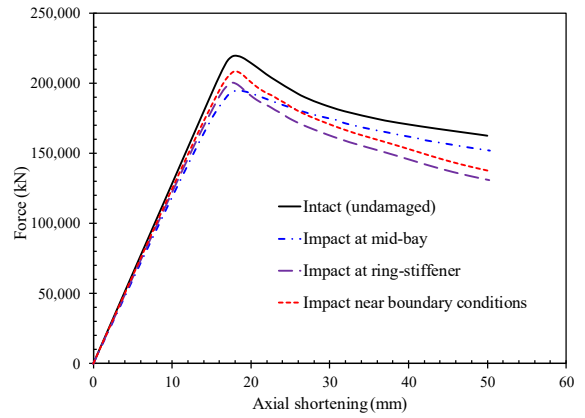


Figure 12. Force-axial shortening relation curve with various impact locations

2.6. Effect of different indenter shape

In actual cases, ring or/and stringer-stiffened cylinder structures are prone to impact in many ways such as a striking ship may collide with these structures by its bow, stern, or side. In this study, three typical striker header shapes as hemisphere type, knife-edge type, and rectangular type have been investigated. The striking ship was modelled as a rigid body. However, in the actual case, the striking ship may also deform due to collision forces. It is noted that the diameter and the width of indenting surfaces are the same as the mid-bay length of the cylinder. The corners of the rectangular and knife-edge indenter were filleted. The first case resembles bulbous bow impact and the second case stern or side impact of a unity vessel and offshore accommodation barge vessel, respectively. For the same impact condition, the numerical results for each type of indenter shape are plotted in Fig. 13. The deformed shapes of each striker type under axial compressive loading are large differences because of the impact contact area.

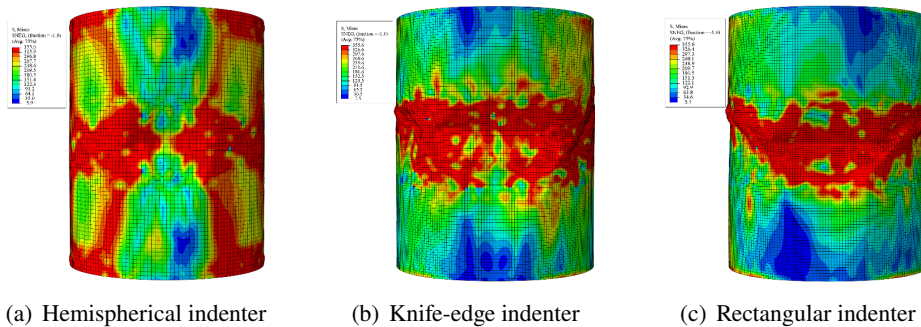


Figure 13. Deformed shape with different indenter surfaces

Furthermore, the residual strength of each case was strongly dependent on striker header shapes. The force-axial shortening relation curve for various striker header shapes was presented in Fig. 14. The most severe case is when the load is applied through a knife-edge indenter. In this case, the ultimate strength reduction when compared with the intact model was 32.6%. When the load is applied through hemisphere type and rectangular type, the ultimate strength reductions when compared with the intact model were 11.4% and 23.8%, respectively.

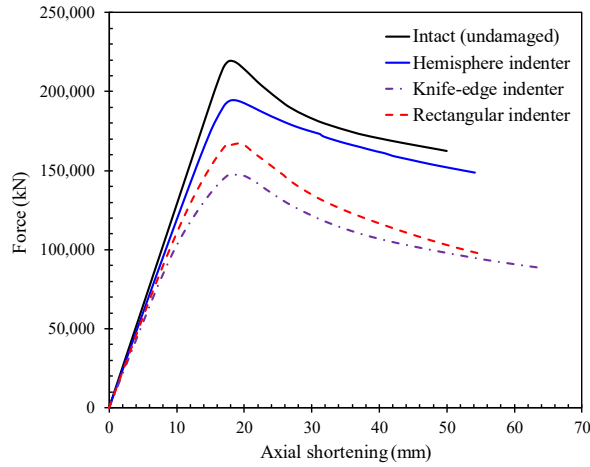


Figure 14. Force-axial shortening relation curve for various striker header shapes

3. Proposed formulation

After investigating the effects of various parameters on the axial compression responses of TLPs in the previous section, the series of parametric studies were performed on actual design scantlings of stringer-stiffened cylinders such as an actual TLPs design concept in the ABS [23]. The details of dimension and material properties were provided in Table 2. For each model, a series of finite element analyses that varied the dent depth were conducted. To generate the damages on models, the collision analysis was conducted using hemisphere indenter. The collision analysis conditions, including the drop height, corresponding collision velocity, striker mass, and kinetic energy of the striker. The impact velocities were 1.0 m/s, 2m/s, 3 m/s, 5.0 m/s, 8 m/s, and 10 m/s. For each velocity, it was performed with a striker mass of 10 tons, 20 tons, and 50 tons, respectively. The range of R/t was

Table 2. Material properties and dimensions of the stringer-stiffened cylinders

Sym.	Unit	SS-1	SS-2	SS-3	SS-4	SS-5	SS-6	SS-7	SS-8
R	mm	3100	3025	2500	4200	3025	13 320	8880	9500
t	mm	28	19.0	15	20.0	12.0	41.5	25.0	20.0
L	mm	12 500	10 240	11 250	10 500	10 240	17 500.0	6600	26 000
L_S	mm	3000	2048.0	2250	3500	2048	3500.0	2200	3200
n_r		4.0	4.0	4.0	2.0	4.0	4.0	2.0	8.0
h_{rw}	mm	210.0	214.0	190.00	700	214.0	787.5	525	650
t_{rw}	mm	25.0	20.0	20	12.0	15.0	37.5	25.0	20.0
b_{rf}	mm	250	200.0	150	300	200	450.0	300	300
t_{rf}	mm	25	20.0	20	16.0	15.0	45.0	30.0	20.0
n_s		20	18.0	20	36	18.0	36.0	60.0	18.0
h_{sw}	mm	130.0	160.0	150	250.0	160.0	450.0	300	400
t_{sw}	mm	25.0	15.0	20	12.0	11.5	37.5	15.0	20.0
w_{sr}	mm	80.0	100.0	100	90.0	100.0	285.0	190.0	200
t_{sf}	mm	25	15.0	20	12.0	11.5	45.0	19.0	20.0
σ_Y	MPa	450	276.0	380	355	276	345.0	345	645
E	GPa	210 000	205 000	206 000	206	205 000	206 000	200 000	207 000
R/t		111	159	167	210	263	321	355	475

determined from 111 to 475. Additionally, the collision of offshore installations with supply vessels is also considered. The impact velocities were 1 m/s, 2m/s and 3 m/s and corresponded to the striker masses were 1000 tons, 3000 tons, 5000 tons, and 7500 tons for the stringer-stiffened cylinders. After generating the impact damages, all models were consequently performed under compressive loadings for assessing the residual strength.

3.1. Design formulations to predict the permanent dent depth

Before deriving equation to predict the residual strength of dented TLPs, the formulations to predict the maximum permanent dent depth were provided as Eqs. (10)–(17). The details of deriving formulation procedures to the maximum permanent dent depth of stringer-stiffened cylinders can be found in Do et al. [24].

$$\delta_d = \frac{d}{R} = 3.59C_S C_L C_\beta (\lambda_E)^{0.68}; \quad \text{Mean equation} \quad (10)$$

$$\delta_d = \frac{d}{R} = 4.16C_S C_L C_\beta (\lambda_E)^{0.68}; \quad \text{Design equation} \quad (11)$$

$$\lambda_E = \frac{E_k}{E_a} \quad (12)$$

$$E_k = \frac{1}{2}mv^2; \quad \text{Kinetic energy} \quad (13)$$

$$E_a = \frac{\sigma_Y + \sigma_T}{2} \varepsilon_T V_{str}; \quad \text{Strain energy absorption capacity} \quad (14)$$

$$V_{Str} = V_{shell} + V_{stringer - stiffener} + V_{ring - stiffener} = AL + V_{stringer - stiffener} + V_{ring - stiffener} \quad (15)$$

$$C_L = \exp\left(-9.91 \frac{x}{L}\right) \quad (16)$$

$$C_\beta = 0.114\beta^2 - 0.346\beta + 1 \quad (17)$$

where C_S is indenter shape factor, in which $C_S = 1$ is hemisphere indenter, $C_S = 0.74$ is knife-edge indenter, $C_S = 0.63$ is rectangular indenter; C_L is impact location factor; C_β is impact angle factor; x is distance from collision to mid-span of ring-stiffened cylinder; L is total length of ring-stiffened cylinder; β is impact angle (rad).

3.2. Proposed formula for dented stringer-stiffened cylinder under axial compression

A series of finite element analysis are performed to evaluate the effect of dent depth on reduction in ultimate strength under axial compression. At one end of the cylinders all degrees of freedom are constrained. All nodes at the other end are tied to a reference point to which an axial displacement is applied. The other five degrees of freedom are constrained. Based on the results of a closed-form formulation may be derived empirically by regression analysis to predict the reduction factor R_u , as indicated in Fig. 15. Once the ultimate strength of an intact cylinder $\sigma_{xu_in.}$ is calculated the residual strength can be obtained by multiplying it by the strength reduction factor. R_u as defined in Eq. (18).

$$R_u = \frac{\sigma_{xu_dam.}}{\sigma_{xu_in.}} = -0.046\left(\frac{d}{R}\right)^2 - 0.59\left(\frac{d}{R}\right) + 1 \quad (18)$$

where R_u is ultimate strength reduction factor; $\sigma_{xu_in.}$ is ultimate strength of intact stringer-stiffened cylinder; $\sigma_{xu_dam.}$ residual strength of dented stringer-stiffened cylinder; d is permanent dent depth (determined by Eq. (10)); R is mean radius of stringer-stiffened cylinder.

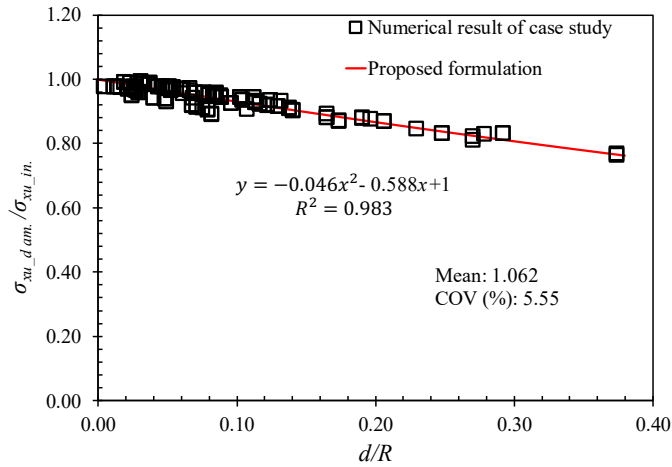


Figure 15. Best-fit curve to predict the residual strength of TLPs

To validate the accuracy and reliability of the proposed formulation for predicting the residual strength of the locally dented steel stringer-stiffened cylinders, the comparisons between the proposed formulation and the available test results in the literature were conducted. For this purpose, the experimental models from Ronalds and Dowling [9] were used. They performed quasi-static denting tests on four small-scale stringer-stiffened cylinders with lateral loading at mid-span, denoted by 3B1, 3B2, 3B3, and 3B4. Then, these models were subsequently loaded axially until collapsed. A comparison of the proposed formulation predictions and available experimental results is summarized in Table 3. The mean of bias (proposed formulation values/test values) was smaller than 11% for all cases. Furthermore, the mean of X_m for all the models was 1.062 together with a COV of 5.55%. It means that the proposed formulation provides a good accuracy for predicting the residual strength of the locally dented steel stringer-stiffened cylinders under compressive loadings.

Table 3. Comparison of the proposed formulation results with the test results

Model	3B1	3B2	3B3	3B4
Test result, σ_{xu_dam} . (MPa)	318	287	277	271
Proposed formulation, σ_{xu_dam} . (MPa)	311	305	304	301
Bias (Prop. formulation/Test), X_m	0.98	1.06	1.10	1.11
Mean	1.062			
COV (%)	5.55			

4. Conclusions

This study aims to investigate the residual strength of locally dented LTPs and deriving equations to predict their residual strength under compressive loadings. There are some findings follows:

- The numerical techniques developed in this study have quite good accuracy when compared to the experimental models from Ronalds and Dowling. However, it should be validated with more available test data.

- In case studies, the extent of local denting damage of the stiffened cylinder was strongly dependent on the impact locations. However, the reduction of ultimate strength with various impact locations was not rapidly decreased as maximum permanent dent depth. The maximum ultimate strength reduction has occurred at mid-bay of ring stiffeners with 7% when compared to impact location near boundary conditions.

- The residual strength of LTPs was strongly dependent on striker header shapes during impact processes. The most severe case is when the load is applied through a knife-edge indenter, while that of hemisphere type is lowest affected on the residual strength of these structures.

- For the first time, the simple design equations to predict the residual strength of the locally dented steel stringer-stiffened cylinders under compressive loadings were successfully conducted in this study. They are convenient to use in the structure's strength of LTPs under risk conditions, during the initial design stage for safety concerns of marine stringer-stiffened cylinder structures.

Acknowledgements

This research is funded by Vietnam National Foundation for Science and Technology Development (NAFOSTED) under grant number 107.01-2019.333.

References

- [1] Cho, S. R., Lee, S. B. (1998). Ultimate strength formulation for stringer-stiffened cylinders subjected to combined axial compression and radial pressure. *International Journal of Ocean Engineering and Technology*, 1(1):41–55.
- [2] Veritas, D. N. (2007). Accident statistics for floating offshore units on the UK continental shelf 1980-2005. *HSE Research Report RR567*. Sudbury, Suffolk HSE Books.
- [3] Do, Q. T., Muttaqie, T., Park, S. H., Shin, H. K., Cho, S. R. (2018). [Predicting the collision damage of steel ring-stiffened cylinders and their residual strength under hydrostatic pressure](#). *Ocean Engineering*, 169:326–343.
- [4] Offshore Technology Report No. OTH/90/329 (1992). *Buckling of offshore structural components Report of the UK Cohesive Buckling Research Programme 1983-1985*. Health and Safety Executive, London (United Kingdom).
- [5] Cho, S. R., Muttaqie, T., Do, Q. T., Kim, S., Kim, S. M., Han, D. H. (2018). [Experimental investigations on the failure modes of ring-stiffened cylinders under external hydrostatic pressure](#). *International Journal of Naval Architecture and Ocean Engineering*, 10(6):711–729.
- [6] Cho, S. R., Muttaqie, T., Do, Q. T., So, H. Y., Sohn, J. M. (2018). [Ultimate strength formulation considering failure mode interactions of ring-stiffened cylinders subjected to hydrostatic pressure](#). *Ocean Engineering*, 161:242–256.
- [7] Cho, S. R., Muttaqie, T., Do, Q. T., Park, S. H., Kim, S. M., So, H. Y., Sohn, J. M. (2019). [Experimental study on ultimate strength of steel-welded ring-stiffened conical shell under external hydrostatic pressure](#). *Marine Structures*, 67:102634.
- [8] Muttaqie, T., Thang, D. Q., Prabowo, A. R., Cho, S. R., Sohn, J. M. (2019). [Numerical studies of the failure modes of ring-stiffened cylinders under hydrostatic pressure](#). *Structural Engineering and Mechanics*, 70(4):431–443.
- [9] Ronalds, B. F., Dowling, P. J. (1986). Buckling of intact and damaged offshore shell structures. In *Advances in Marine Structures Conference*, Dunfermline, UK, 201–218.
- [10] Harding, J. E., Onoufriou, A. (1995). [Behaviour of ring-stiffened cylindrical members damaged by local denting](#). *Journal of Constructional Steel Research*, 33(3):237–257.
- [11] Walker, A. C., McCall, S., Thorpe, T. W. (1987). [Strength of damage ring and orthogonally stiffened shells—Part I: Plain ring stiffened shells](#). *Thin-Walled Structures*, 5(6):425–453.

- [12] Walker, A. C., McCall, S., Thorpe, T. W. (1988). [Strength of damaged ring and orthogonally stiffened shells—Part II: T-ring and orthogonally stiffened shells](#). *Thin-Walled Structures*, 6(1):19–50.
- [13] Do, Q. T., Muttaqie, T., Shin, H. K., Cho, S. R. (2018). [Dynamic lateral mass impact on steel stringer-stiffened cylinders](#). *International Journal of Impact Engineering*, 116:105–126.
- [14] Do, Q. T., Muttaqie, T., Park, S. H., Shin, H. K., Cho, S. R. (2018). [Ultimate strength of intact and dented steel stringer-stiffened cylinders under hydrostatic pressure](#). *Thin-Walled Structures*, 132:442–460.
- [15] Do, Q. T., Muttaqie, T., Park, S. H., Shin, H. K., Cho, S. R. (2019). [Residual strength of dented stiffened cylinders under combined loads](#). In *Proceeding of Progress in the Analysis and Design of Marine Structures*, Dubrovnik, Croatia, CRC Press, 116–125.
- [16] Do, Q. T., Le, D. N. C., Seo, B. S., Shin, H. K., Cho, S. R. (2019). [Fracture response of tubular T-joints under dynamic mass impact](#). In *International Conference on Collision and Grounding of Ships and Offshore Structures*, Lisbon, Portugal, CRC Press, 75–84.
- [17] Do, Q. T., Muttaqie, T., Park, S. H., Shin, H. K., Cho, S. R. (2018). Residual strength of stringer-stiffened cylinder subjected to external hydrostatic pressure. In *Proceeding of the 3rd International Conference on Safety And Reliability of Ships-Offshore & Subsea Structures*, Wuhan University of Technology, China.
- [18] Do, Q. T., Muttaqie, T., Shin, H. K., Cho, S. R. (2017). On the resistance of stringer-stiffened cylinders subjected to dynamic lateral mass impact. In *Proceeding of the 31th Asian-Pacific Technical Exchange and Advisory Meeting on Marine Structures (TEAM)*, Osaka, Japan.
- [19] Do, Q. T., Park, S. H., Shin, H. K., Cho, K. N., Cho, S. R. (2018). Ultimate strength formulations of intact and dented ring-stiffened cylinders under external hydrostatic pressure. In *Proceeding of the 32th Asian-Pacific Technical Exchange and Advisory Meeting on Marine Structures (TEAM)*, Wuhan University of Technology, China.
- [20] Do, Q. T., Muttaqie, T., Park, S. H., Shin, H. K., Cho, S. R. (2018). [Predicting the collision damage of steel ring-stiffened cylinders and their residual strength under hydrostatic pressure](#). *Ocean Engineering*, 169:326–343.
- [21] Cho, S. R., Do, Q. T., Shin, H. K. (2017). [Residual strength of damaged ring-stiffened cylinders subjected to external hydrostatic pressure](#). *Marine Structures*, 56:186–205.
- [22] Viet, V. Q., Ha, H., Hoan, P. T. (2019). [Evaluation of ultimate bending moment of circular concrete-filled double skin steel tubes using finite element analysis](#). *Journal of Science and Technology in Civil Engineering (STCE)-NUCE*, 13(1):21–32.
- [23] American Bureau of Shipping (2018). *Guide for buckling and ultimate strength assessment for offshore structures*. Houston, TX, USA.
- [24] Do, Q. T., Huynh, V. V., Tuyen, V. V., Pham Thanh, N., Tra, T. H., Vu, Q. V., Cho, S. R. (2020). [A new formulation for predicting the collision damage of steel stiffened cylinders subjected to dynamic lateral mass impact](#). *Applied Sciences*, 10(11):3856.
- [25] Das, P. K., Subin, K. K., Pretheesh, P. C. (2011). A revisit on design and analysis of stiffened shell structures for offshore applications. In *Proceedings of the 3rd International Conference on Marine Structures (MARSTRUCT 2011)*, Hamburg, Germany, 119–131.
- [26] API (2004). *Bulletin on stability design of cylindrical shells*. API Bulletin 2U, 3rd ed., Washington.
- [27] Xiong, Z., Hui, H., Huang, Z. (2020). [The ultimate strength of ring stiffened cylindrical shell and its influence factors](#). *Journal of Theoretical and Applied Sciences*, 3:15.